hsa_circNFXL1_009 modulates apoptosis, proliferation, migration, and potassium channel activation in pulmonary hypertension

Xin Jin,[1,8] Yuanyuan Xu,[2,8] Min Guo,[3] Yushuang Sun,[4] Junzhu Ding,[4] Lu Li,[1] Xiaodong Zheng,[5] Shuzhen Li,[6] Dandan Yuan,[7] and Shan-Shan Li[1]

[1]School of Medicine, Nankai University, Tianjin, China; [2]Department of Cardiology, The Fourth Affiliated Hospital of Harbin Medical University, Harbin, China; [3]Department of Endocrinology, The Fourth Affiliated Hospital of Harbin Medical University, Harbin, China; [4]Department of Biopharmaceutical Sciences, College of Pharmacy, Harbin Medical University, Harbin, China; [5]Department of Genetics and Cell Biology, Harbin Medical University-Daqing, Daqing, China; [6]Department of Immunology, College of Basic Medical Sciences, Shenyang Medical College, Shenyang, China; [7]Department of Gynecology and Obstetrics, The Second Affiliated Hospital of Harbin Medical University, Harbin, China

In this study, we explored the circular RNA (circRNA) profile in pulmonary arterial hypertension (PAH) patients caused by chronic obstructive pulmonary disease (COPD) and the effects of hsa_circNFXL1_009 on abnormal proliferation, apoptosis, and migration of human pulmonary arterial smooth muscle cells (hPASMCs) driven by hypoxia. Using microarrays, we screened the circRNA profile in whole-blood samples from three pairs of subjects and found 158 dysregulated circRNAs in patients with PAH-COPD. Quantitative reverse transcriptase polymerase chain reaction (qRT-PCR) analysis further validated that hsa_circNFXL1_009 was dramatically downregulated with the highest area under a receiver operating characteristic curve (ROC) in 21 pairs of subjects. Consistently, exposure to hypoxia markedly reduced the hsa_circNFXL1_009 level in cultured hPASMCs. Delivery of exogenous hsa_circNFXL1_009 attenuated hypoxia-induced proliferation, apoptotic resistance, and migration of hPASMCs, as evidenced by immunocytochemistry, 5-ethynyl-2′-deoxyuridine incorporation, wound healing, and a TUNEL (terminal deoxynucleotidyl transferase-mediated deoxyuridine triphosphate nick end labeling) assay. A luciferase assay showed that hsa_circNFXL1_009 directly sponged hsa-miR-29b-2-5p (miR-29b) and positively regulated the expression of voltage-gated potassium (K^+) channel subfamily B member 1 (_KCNB1_) at the mRNA level. Using patch-clamp electrophysiology, we proved that overexpression of hsa_circNFXL1_009 promoted a whole-cell K^+ current in hPASMCs. Taken together, these studies identify hsa_circNFXL1_009 as a key regulator of PAH, and it may be used as a potential therapeutic target for the treatment of PAH.

INTRODUCTION

Pulmonary arterial hypertension (PAH) is a malignant and progressive disease characterized by remodeling and obstructions of the pulmonary arteries (PAs), which are mainly due to the proliferation of vasculature and excessive PA contraction. The resultant PAH causes continuous increases in pulmonary circulation resistance and PA pressure, eventually leading to right ventricular failure and death.[1–3] Although the precise mechanisms for pulmonary arterial obstructions are still unclear, the imbalance between proliferation and apoptosis of pulmonary arterial smooth muscle cells (PASMCs) as well as abnormal PASMC migration are well known to be involved in PA remodeling during the development of PAH.[4]

A unique feature of PASMCs is their response to hypoxia. Instead of vasodilation in the systemic circulation, hypoxia produces vasoconstriction in pulmonary circulation.[5] Thus, hypoxia is widely used to initiate PAH in animal models and cultured PASMCs. In these experimental models, hypoxia has anti-apoptotic and pro-proliferative effects on PASMCs, which subsequently cause PASMC migration, remodeling of pulmonary vessel walls, and vascular constriction. Indeed, accumulating experimental evidence from the hypoxic models indicates that dysregulation of certain cellular signaling molecules is critical for PASMC proliferation.[6]

Among these cellular signaling molecules, there are the newly demonstrated non-coding RNAs other than classic mRNAs, tRNAs, and rRNAs. Circular RNAs (circRNAs) are a novel class of non-coding RNAs that are often produced as side products of mRNA editing and splicing.[7] Unlike linear RNAs, circRNAs are generated by RNA back splicing and are characterized by a closed loop structure with a covalent bond linking the 3′ and 5′ terminus. The circRNAs express

highly stable, conserved, tissue-specific, and stage-dependent patterns across species.[8,9] Although the functional significance of most circR-NAs remains elusive, some circRNAs have recently been shown to participate in the biological processes (BPs) of the cell. A well-demonstrated function of the circRNAs is to serve as microRNA (miRNA) inhibitors by sequestering miRNAs, which can affect the expression and decay of mRNAs, a process known as miRNA sponging.[10] Additionally, circRNAs may be involved in recruiting other RNA species and proteins, encoding peptides or proteins with their endogenous open-reading frame sequences, and sequestering proteins in the cytoplasm.[11–14] Previous studies have shown that circRNAs play an important role in neurological diseases, atherosclerosis, prion diseases, and various cancers by regulating cell cycle progression, proliferation, apoptosis, and tumorigenesis.[15–23] In the PASMCs, some circRNAs have pro-proliferation effects that increase cell viability and decrease cells arrested in the G_1/G_0 phase.[24]

In addition to pro-proliferation, certain circRNAs may have an antiproliferation function. The understanding of the latter may lead to new information on PAH development and prevention. With this reasoning, we hypothesized that aberrant expression of circRNAs might play an essential role in the pathophysiology of PAH. Thus, in this study, we aimed to determine the expression pattern of circRNAs in whole-blood samples from patients with PAH caused by chronic obstructive pulmonary disease (COPD) and to investigate the role of circRNA in hypoxic hPASMCs. We report for the first time that overexpression of hsa_circNFXL1_009 decreases excessive proliferation, apoptotic resistance, and migration of hPASMCs under hypoxic conditions. hsa_circNFXL1_009 also sponges hsa-miR-29b-2-5p, inhibits voltage-gated potassium (K^+) channel subfamily B member 1 (*KCNB1*) gene expression at the mRNA level, and increases the K^+ channel current in hPASMCs, providing Competing endogenous RNA (ceRNA) mechanisms underlying hsa_circNFXL1_009-regulated pathogenesis of PAH.

RESULTS

Differential circRNA expression profile in PAH-COPD patients

circRNA profiling was performed with an Arraystar human circRNA array in three pairs of subjects. We set a cutoff value for differential expression fold change to 1.5 and found 158 significantly dysregulated circRNAs (27 upregulated and 131 downregulated) in the PAH-COPD patients (Figure 1A, p < 0.05, false discovery rate [FDR] < 0.05). Among these differentially expressed circRNAs, most downregulated circRNAs came from chromosomes 2 (chr2), 3 (chr3), and 7 (chr7), whereas the upregulated circRNAs were scattered over all chromosomes (Figure 1B). Moreover, most of these circRNAs were generated from the protein-coding exons (84% of downregulated circRNAs and 89% of upregulated circRNAs) (Figure 1C). The hierarchical cluster analysis revealed that the circRNA expression patterns were distinctive between PAH-COPD and control subjects (Figures 1D and 1E).

Validation of the most distinctive circRNAs in PAH-COPD patients

From microarray results, we selected the top 20 most differentially expressed circRNAs for validation in 21 pairs of subjects. The qRT-PCR

results showed that five circRNA expression trends were consistent with microarray results, which included hsa_circNFXL1_009, hsa_circMFN2_004, has_circ_ZNF302, hsa_circGSDMD_004, and hsa_circWDR37_016 (Figures 2A–2E). To assess the performance of these five circRNAs in predicting potential association with PAH, we calculated their receiver operating characteristic (ROC) curves and evaluated their accuracy with determination of the area under the ROC curve (AUC). The highest AUC value was for hsa_circNFXL1_009 (AUC, 0.9410; 95% confidence interval [CI], 0.8653–1.000; p < 0.0001) (Figure 2F), and was followed by has_circ_ZNF302 (AUC, 0.8476; 95% CI, 0.7279–0.9673; p < 0.001) (Figure 2H); hsa_circWDR37_016 (AUC, 0.8225; 95% CI, 0.6916–0.9534; p < 0.001) (Figure 2J); hsa_circMFN2_004 (AUC, 0.7472; 95% CI, 0.5989–0.8955; p < 0.01) (Figure 2G); and hsa_circGSDMD_004 (AUC, 0.7316; 95% CI, 0.5703–0.8929; p < 0.05) (Figure 2I). As hsa_circNFXL1_009 was the most significantly downregulated circRNA in 21 PAH-COPD patients with the highest AUC value, we next focused on investigating its roles in PAH pathogenesis.

hsa_circNFXL1_009 in the regulation of hPASMC apoptosis, proliferation, and migration

As hypoxia is a well-recognized risk factor for PAH, and hypoxic pulmonary arterial remodeling in PAH is mainly driven by abnormal proliferation, apoptotic resistance, and migration of PASMCs, we further investigated the role of hsa_circNFXL1_009 in response to hypoxia in cultured hPASMCs. First, we verified the formation of hsa_circNFXL1_009 in hPASMCs. As shown in Figure 3A, hsa_circNFXL1_009 is generated from the *NFXL1* gene located on human chromosome 4 (chr4; 47905210-47907363), with no homology in the mouse. The head-to-tail splicing site was assayed by RT-PCR with convergent and divergent primers (Figure 3B). Sanger sequencing further confirmed the head-to-tail junction, which was consistent with hsa_circNFXL1_009 annotation (Figure 3C). Using RNA fluorescence *in situ* hybridization (FISH), we confirmed the expression of hsa_circNFXL1_009 in hPASMCs (Figures 3D–3F). Consistent with the results in patients with PAH-COPD, hsa_circNFXL1_009 was markedly downregulated by hypoxia in a time-dependent manner in hPASMCs (Figures 3G and 3H).

Subsequently, we constructed a circRNA expression vector to overexpress hsa_circNFXL1_009 in hPASMCs (Figure S1) and assessed its effects on cell viability, migration, apoptosis, and proliferation under hypoxic conditions. As shown in Figure 4, hsa_circNFXL1_009 overexpression reversed the hypoxia-induced increase in migration and proliferation of hPASMCs (as measured by wound healing, 5-ethynyl-2′-deoxyuridine [EdU] incorporation, and Ki67 staining). Also, hsa_circNFXL1_009 overexpression attenuated hypoxia-induced anti-apoptosis effects (as measured by TUNEL assay), indicating a protective role of hsa_circNFXL1_009 in hypoxic pulmonary vascular remodeling (HPVR).

hsa_circNFXL1_009 acts as an hsa-miR-29b-2-5p sponge

By targeting MREs, circRNAs can regulate mRNA by competitive sponging its miRNAs. Bioinformatics was used to construct the
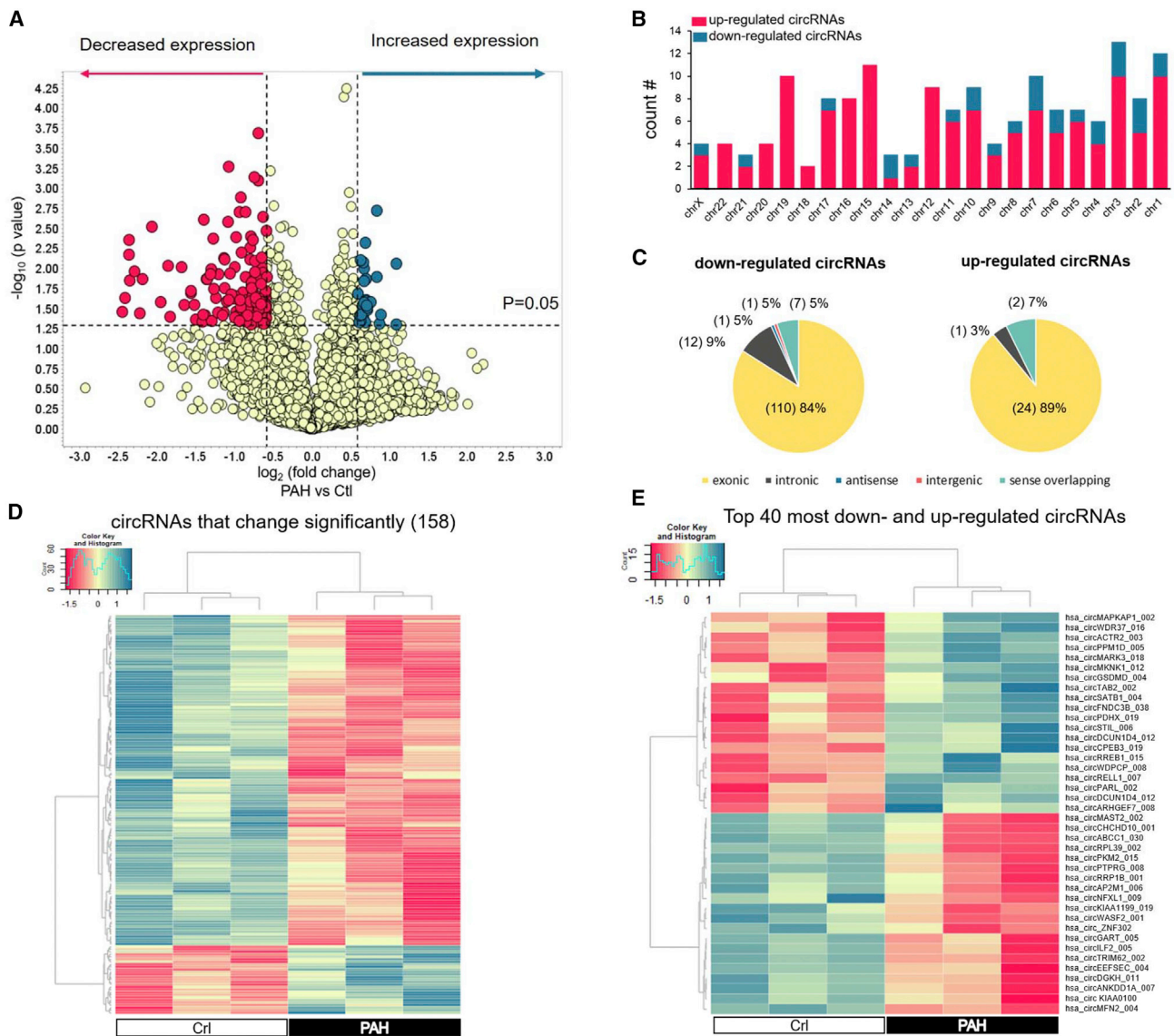
Figure 1. circRNA profile, the genome-wide landscape view, and hierarchical clustering of PAH-COPD patients and healthy controls

(A) Volcano plot shows the different expression of circRNAs in two groups of subjects. Red/green dots indicate circRNAs expressed more/less than a 1.5-fold change in PAH-COPD patients. (B) Numbers of dysregulated circRNAs coming from different chromosomes. (C) Pie chart represents the percentage of dysregulated circRNAs coming from different chromosome regions. (D) Heatmap of 158 most significantly dysregulated circRNAs. (E) Heatmap of the top 40 dysregulated circRNAs (20 upregulated and 20 downregulated). Green/red represent a low/high expression level. PAH-COPD, pulmonary arterial hypertension due to chronic obstructive pulmonary disease; circRNA, circular RNA. n = 3 pairs of subjects. Comparisons of data were acquired by a Student's t test.

hsa_circNFXL1_009-miRNAs-mRNAs network to find the potential targets of hsa_circNFXL1_009. In this ceRNA module, circRNA-miRNA-mRNA interactions showed the potential actions of hsa_circNFXL1_009 as sponges for miRNAs, and thus affecting the expression of targeted genes (Figure S2). In the prediction, the top five miRNAs for hsa_circNFXL1_009 sponging were hsa-miR-210, hsa-miR-29-2-5p, hsa-miR-381-3p, hsa-miR-300, and hsa-let-7 (Figure 5A). Also, DIANA-miRPath analysis revealed that these five miRNAs were related to the cellular nitrogen compound metabolic

process and transforming growth factor (TGF)-β signaling pathway (Figures S3A and S3B). The Gene Ontology (GO) analysis indicated that the BPs were the regulation of monocyte chemotactic protein-1 (MCP-1) production, mRNA transcription from the RNA polymerase II promoter, and mRNA transcription. The top three GO terms in the molecular function (MF) category were β-amyloid binding, catalytic activity, and motor activity. The top three GO terms in the cellular component (CC) were ciliary tip, ciliary plasm, and axoneme. Additionally, Kyoto Encyclopedia Genes and Genomes (KEGG)
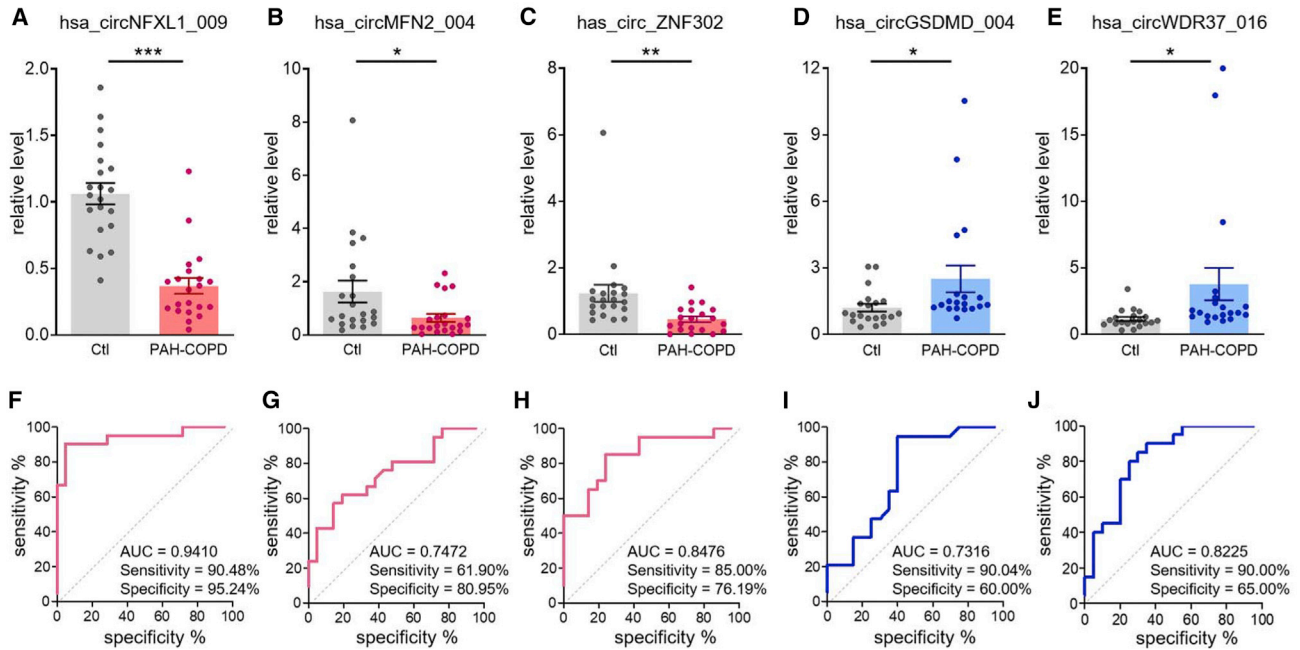
Figure 2. Validation and evaluation of differentially expressed circRNAs

(A–E) hsa_circNFXL1_009 (A), hsa_circMFN2_004 (B), and hsa_circ_ZNF302 (C) were significantly downregulated, while hsa_circGSDMD_004 (D) and hsa_circWDR37_016 (E) were significantly upregulated in patients with PAH-COPD. (F–J) ROC curve analysis of validated five circRNAs showing their performance in predicting potential association with PAH-COPD. qRT-PCR, quantitative reverse transcriptase polymerase chain reaction; AUC, the area under the receiver operating characteristic (ROC) curve. *p < 0.05, **p < 0.01, ***p < 0.001 (n = 21 pairs of subjects). Comparisons of data were acquired by a Student's t test.

analysis indicated the related pathways and associated functions. Four KEGG pathways for the target genes of hsa_circNFXL1_009 involved the nuclear factor κB (NF-κB) signaling pathway, indicating the role of hsa_circNFXL1_009 in inflammatory PAH (Figure S3C).

Among the top five predicted miRNAs, we focused on hsa-miR-210 and hsa-miR-29-2-5p, as they are PAH-related miRNAs.[25–28] Bioinformatics analysis showed that there were two seven-seed nucleotide regions at the positions 100–106 and 58–64 of hsa_circNFXL1_009 matching the hsa-miR-29b-2-5p and hsa-miR-210-5p, respectively. We made several constructs to demonstrate their potential interactions (Figure 5B). As shown in Figure 5C, hsa-miR-29b-2-5p significantly reduced wild-type hsa_circNFXL1_009 (circNFXL1-WT) luciferase activity, whereas this effect was abrogated when the hsa-miR-29b-2-5p binding site in region 100–106 of hsa_circNFXL1_009 (circNFXL1-M1) was mutated. In contrast, the hsa-miR-210-5p had no effects on either circNFXL1-WT or mutated (in region 44–67) hsa_circNFXL1_009 (circNFXL1-M2) (Figure 5D).

To further understand the regulation of hsa-miR-29b-2-5p expression by hsa_circNFXL1_009, we overexpressed hsa_circNFXL1_009 in hPASMCs under hypoxic conditions. hPASMCs transfected with empty vector (pLC) and cultured under normal (Nor-pLC)/hypoxic (Hyp-pLC) conditions served as controls. In comparison with normal hPASMCs, the expression of hsa-miR-29b-2-5p in hPASMCs was greatly induced by hypoxia, and hsa_circNFXL1_009 transfection

(Hyp-circNFXL1) significantly inhibited this increase, indicating an inverse correlation between hsa_circNFXL1_009 and hsa-miR-29b-2-5p expression under hypoxic conditions (Figure 5E).

hsa_circNFXL1_009 in regulation of KCNB1 expression and whole-cell K⁺ current in hPASMCs

Bioinformatics screening (http://www.mirdb.org;https://sfold.wadsworth.org/starmirDB.php suggested that KCNB1, a member in the voltage-gated K⁺ subtype 2.1 (Kv2.1), was one potential target gene of hsa-miR-29b-2-5p with four complementary binding sites located in the 3′ UTR and coding sequence (CDS) region of the KCNB1 gene (Figure 6A). The hypoxia-sensitive K⁺ channel expression and activity were suppressed in PASMCs from humans with PAH.[29–31] Loss of Kv2.1 in PASMCs leads to a sustained depolarization that increases intracellular calcium and K⁺, thereby contributing to proliferation and apoptotic resistance of PASMCs in the pathogenesis of PAH.[32] Therefore, we overexpressed hsa_circNFXL1_009 in hPASMCs and cultured it under hypoxic conditions to study its effects on KCNB1 gene expression. hPASMCs transfected with empty vector (pLC) and cultured under normal (Nor-pLC)/hypoxic (Hyp-pLC) conditions served as controls. In comparison with normal hPASMCs, the mRNA level of the KCNB1 gene in hPASMCs was suppressed greatly by hypoxia, and hsa_circNFXL1_009 transfection (Hyp-circNFXL1) significantly reversed this hypoxia-induced inhibition, indicating that hsa_circNFXL1_009 mediated suppressed K⁺ channel expression in PAH (Figure 6B). Next, we investigate whether
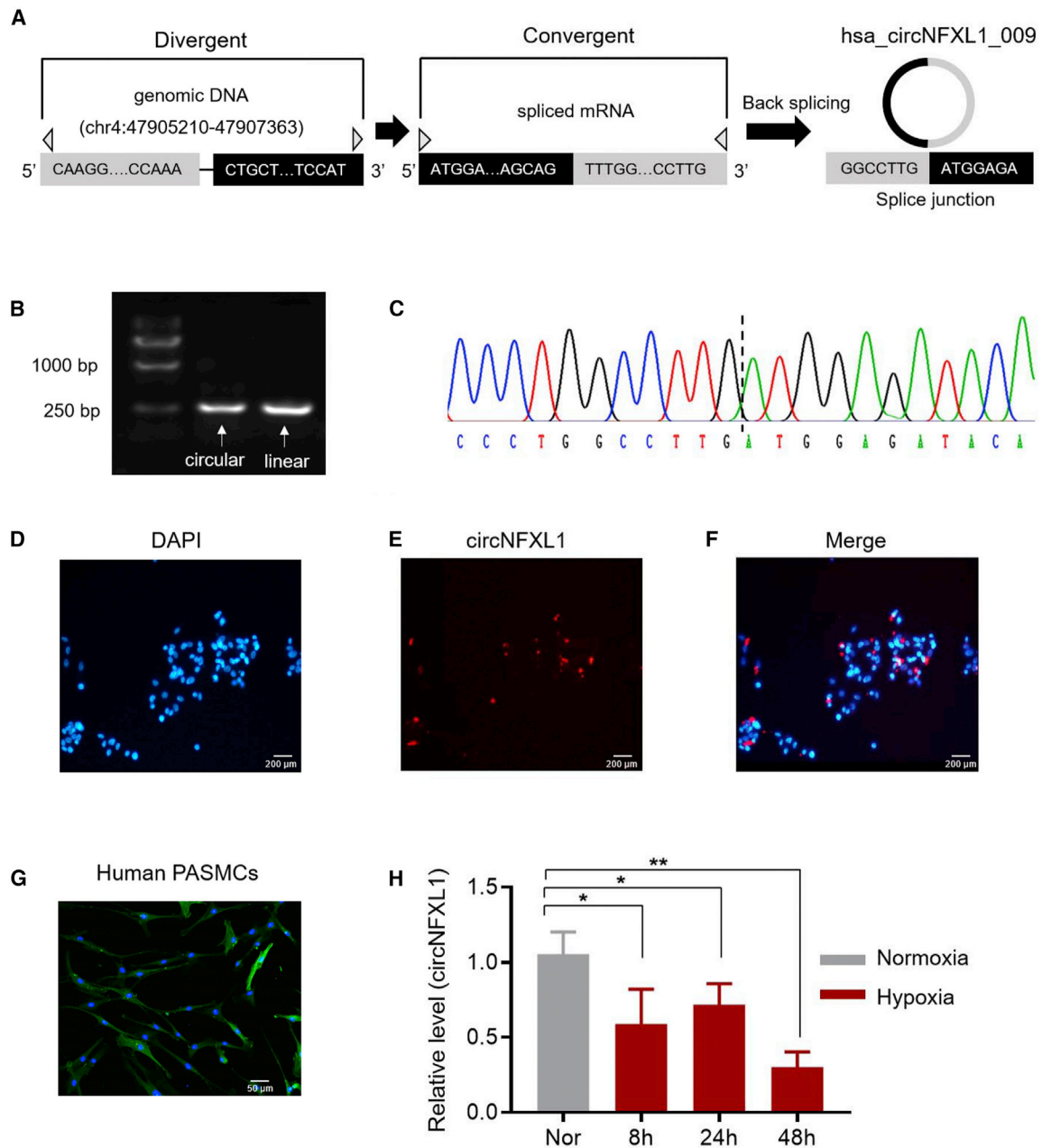
Figure 3. Identification of hsa_circNFXL1_009 in human pulmonary arterial smooth muscle cells (hPASMCs)

(A) Annotation of hsa_circNFXL1_009. (B and C) RT-PCR and sequencing analysis of head-to-tail splicing junction of hsa_circNFXL1_009 in hPASMCs. (D–F) FISH analysis of hsa_circNFXL1_009 in hPASMCs. (G) α-Smooth muscle actin staining in cultured hPASMC cell lines. hPASMCs were fixed, permeabilized, blocked, and incubated with the anti-α-smooth muscle actin antibody (FITC) and imaged with a confocal microscope (shown in yellow). Nuclei were labeled with DAPI (shown in blue). (H) qRT-PCR analysis of hsa_circNFXL1_009 in hPASMCs followed by exposure to hypoxia for different time courses. *p < 0.05, **p < 0.01 (n = 6 individual experiments from four primary hPASMC lines). Comparisons of data were acquired by one-way ANOVA followed by a Bonferroni post hoc test.

hsa_circNFXL1_009 had a significant effect on the K^+ current in hPASMCs. After a 24-h transfection of hsa_circNFXL1_009 (circNFXL1) or empty vector (pLC) under normal conditions, the whole-cell K^+ currents were elicited by depolarizing the hPASMCs from the range of −80 to +90 mV at a holding potential of −70 mV. As shown in Figures 6C–6E, overexpression of hsa_circNFXL1_009 increased the whole-cell K^+ channel currents in hPASMCs. It induced a remarkable shift in the slope of the current-voltage (I-V) curve and significantly increased the amplitude of K^+ currents. The average amplitude of K^+ currents in the
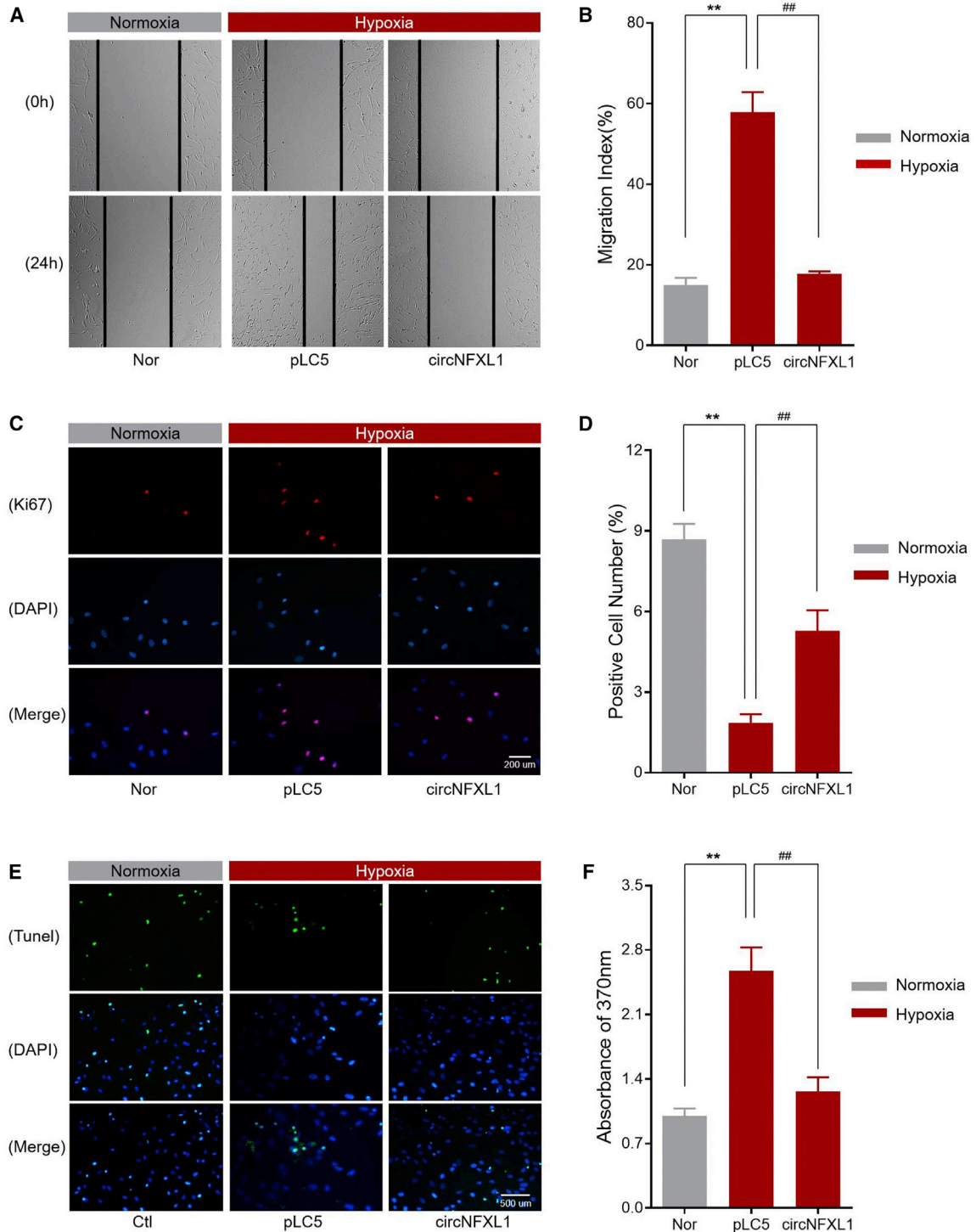
Figure 4. Effects of hsa_circNFXL1_009 on hypoxia-induced hPASMC proliferation and anti-apoptosis

hPASMCs were transfected with pLC5-ciR (pLC5) or hsa_circNFXL1_009 (circNFXL1) and cultured under normal/hypoxic conditions for 48 h. hPASMCs transfected with pLC5-ciR and cultured under normal conditions were used as controls (Nor). (A and B) Cellular migration experiments of hPASMCs transfected and cultured as indicated. (C and F) Ki67 staining was performed by immunofluorescence. (D and E) TUNEL assay of hPASMCs transfected and cultured as indicated. **p < 0.01, ##p < 0.01 (n = 4–6 individual experiments; at least 6–10 fields from each group were imaged and scored in a blinded fashion). Comparisons of data were acquired by one-way ANOVA followed by a Bonferroni post hoc test.
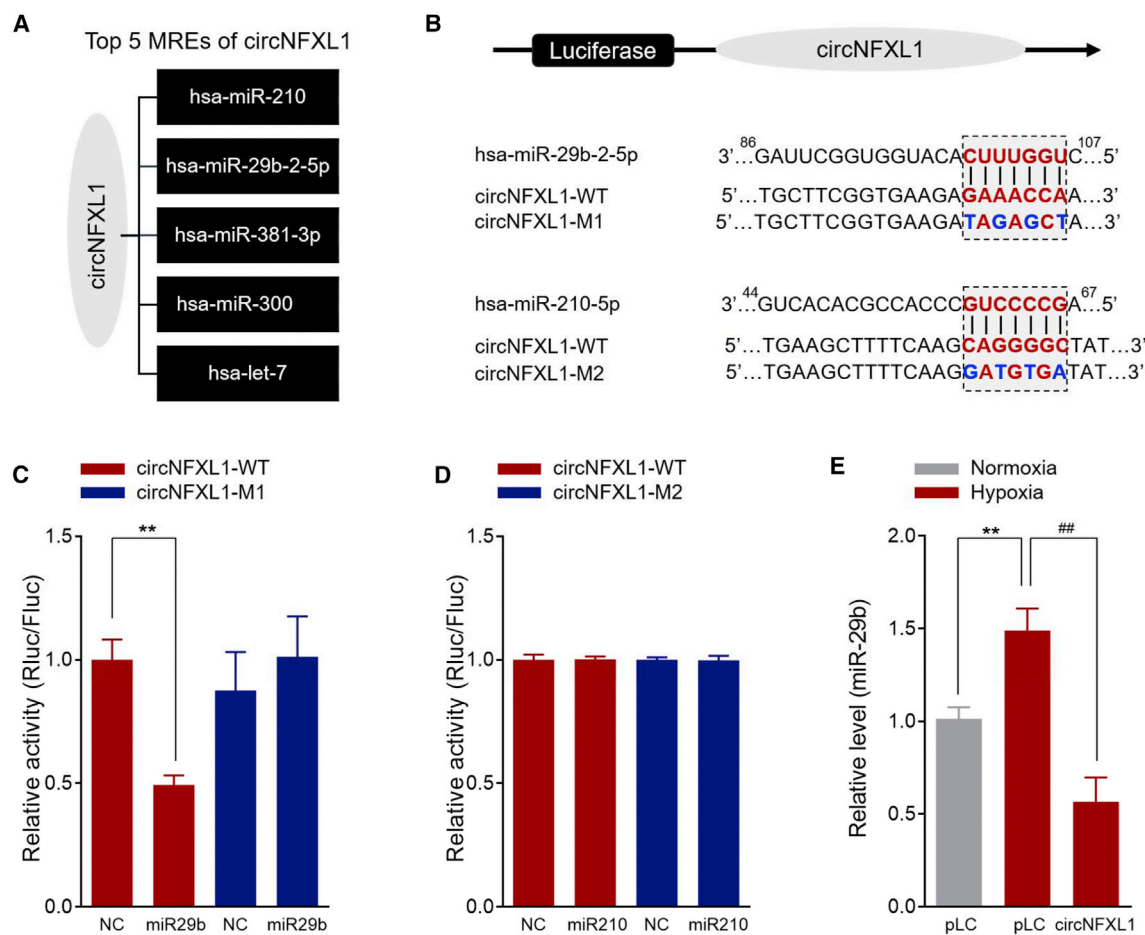
Figure 5. Validation of miRNAs for hsa_circNFXL1_009 sponging

(A) Predicted top five miRNAs for hsa_circNFXL1_009 by ceRNA analysis. (B) Structure diagram of luciferase reporter of hsa_circNFXL1_009 and its mutants. Seed match regions of hsa_circNFXL1_009 and miRNAs are indicated as vertical lines. The mutation sites in hsa_circNFXL1_009 are indicated in blue. (C and D) Luciferase assay for hsa_circNFXL1_009. hsa-miR-29b-2-5p (miR29b)/hsa-miR-210-5p (miR210) mimics were co-transfected with wild-type hsa_circNFXL1_009 (circNFXL1-WT) or its mutations (circNFXL1-M1/circNFXL1-M2) into 293 cells. Luciferase activities were measured after 1 day of culture (n = 3 individual experiments). (E) qRT-PCR analysis of hsa-miR-29b-2-5p in hPASMCs transfected with hsa_circNFXL1_009 expression vector and cultured under hypoxic conditions for 48 h (circNFXL1). hPASMCs transfected with pLC5-ciR and cultured under normal/hypoxic conditions were used as controls (Nor-pLC/Hyp-pLC). $**p < 0.01$, $\#\#p < 0.01$ (n = 5 individual experiments). Comparisons of data were acquired by a Student's t test or a one-way ANOVA followed by a Bonferroni post hoc test.

circNFXL1-transfected cells at +80 mV was 17.2 ± 3.1 compared to 9.8 ± 2.1 (pA/pF) in the cells transfected with empty vector (p < 0.05). These molecular and electrophysiology data proved that hsa_circNFXL1_009 regulated K^+ channel expression and the whole-cell K^+ current in hPASMCs. By regulating K^+ channel expression and activities, hsa_circNFXL1_009 may exert its function in PAH via targeting the hsa-miR-29b-2-5p-KCNB1 axis.

DISCUSSION

PAH is a common complication of COPD with high prevalence and poor survival. Effective treatments of PAH are rare, especially those focused on endogenous mechanisms. Circulating non-coding RNAs are endogenous molecules that are relatively stable and accessible for diagnosis, therapy, and prognosis. In the present study, we have shown

a novel circRNA, hsa_circNFXL1_009, with a distinctive expression pattern in PAH-COPD patients and that is downregulated by hypoxia in hPASMCs. We present novel data demonstrating that hsa_circNFXL1_009 modulates hypoxia-induced apoptosis, proliferation, and migration of hPASMCs, thereby regulating K^+ channel expression and currents in hPASMCs. Mechanistically, these seem to be mediated via the hsa_circNFXL1_009-hsa-miR-29-2-5p-KCNB1 axis.

Recent studies indicate that circRNAs act as critical regulators in various diseases. Some circRNAs are so abundant in the cytoplasm that they exceed their associated linear mRNAs by >10-fold.[33] Unlike the linear non-coding RNAs, their stable structure, specific expression pattern, and high conservation suggest their roles as potential biomarkers for diagnostic, therapeutic, and prognostic purposes.
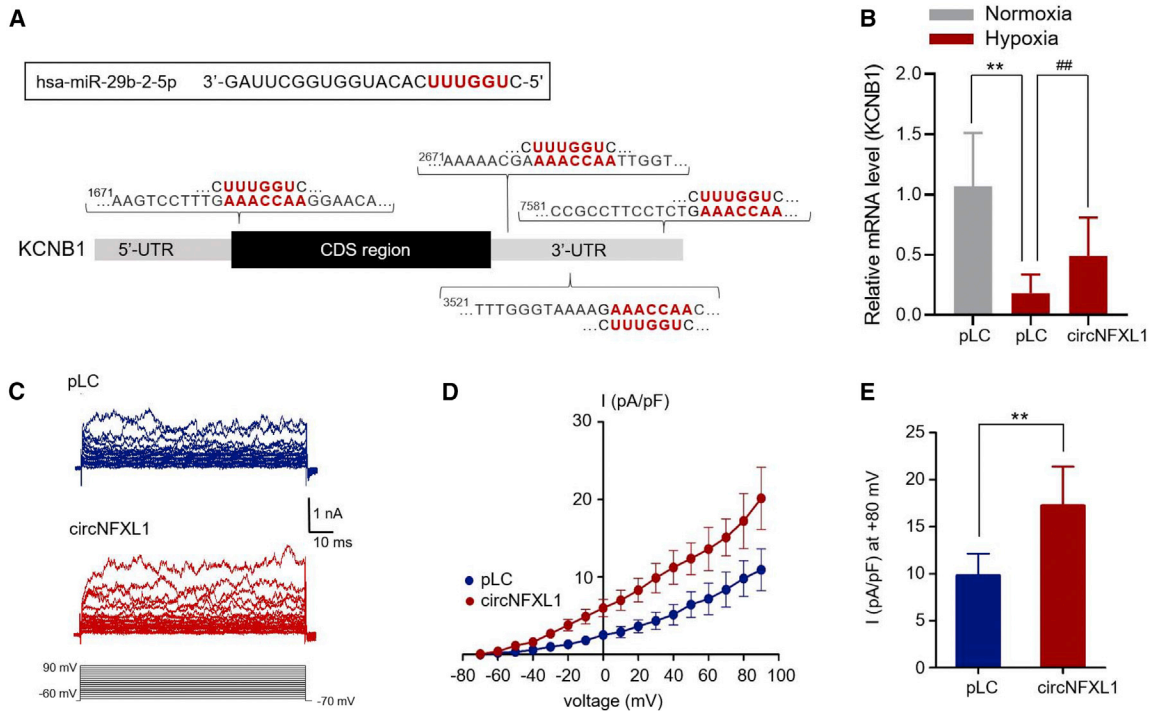
Figure 6. Overexpression of hsa_circNFXL1_009 increased K⁺ channel activities in hPASMCs

(A) Bioinformatics prediction of three complementary binding sites between hsa-miR-29b-2-5p and the 3′ UTR/CDS region of KCNB1. Seed locations in the 3′ UTR were numbered starting from the 3′ UTR, and the seed location in the CDS region was numbered starting from the start codon. (B) Overexpression of hsa_circNFXL1_009 increased the expression of KCNB1 in the mRNA level under hypoxia conditions. hPASMCs were transfected with pLC5-ciR (pLC) or hsa_circNFXL1_009 (circNFXL1) and cultured under hypoxic conditions for 48 h (hyp-circNFXL1). hPASMCs transfected with pLC5-ciR and cultured under normal/hypoxic conditions were used as controls (Nor-pLC/Hyp-pLC) (n = 6 individual experiments). (C) Representative traces recorded with whole-cell voltage clamp in the circNFXL1 vector (circNFXL1)- or empty vector (pLC)-transfected hPASMCs. (D) The current-voltage (I-V) curve from two groups of hPASMCs was analyzed at a steady-state of the voltage-dependent currents (150–180 ms). (E) The average amplitude of K⁺ currents recorded at +80 mV was compared between two groups of hPASMCs. **p < 0.01, ##p < 0.01 (n = 8 cells for circNFXL1, and n = 8 cells for empty vector-transfected hPASMCs from three individual experiments). Comparisons of data were acquired by a one-way ANOVA followed by a Bonferroni post hoc test or a Student's t test.

In our study, we demonstrated the aberrant expression of circRNAs in PAH-COPD patients and provided groups of candidates that were upregulated and downregulated. Chromosome categorization revealed that the upregulated circRNAs were generated from exons in various chromosomes, including sex chromosomes. However, the distributions of the downregulated circRNAs were more specific for chr2, chr3, and chr7. As sequences of circRNAs dedicate their actions to target genes, the distributions of the dysregulated circRNAs may reflect the effects of circRNAs on BPs.

In this study, we confirmed for the first time that hsa_circNFXL1_009 is expressed in hPASMCs, downregulated by hypoxia, and participates in PASMC proliferation, migration, and anti-apoptosis, indicating its role in HPVR observed in PAH. The hsa_circNFXL1_009-miRNAs-mRNAs network revealed that each miRNA (hsa-miR-210-5p, hsa-miR-300, hsa-miR-29b-2-5p, hsa-miR-381-3p, and hsa-let-7f-2-3p) was bound by hsa_circNFXL1_009, which in turn regulated the miRNA-targeted genes. Remarkably, miR-210 is a hypoxia-inducible miRNA, and it has an anti-apoptotic

effect in PASMCs in hypoxia-induced PAH mice.[32] Additionally, the miR-29 family members are highly conserved across species and expressed in the adult mouse lung, playing a role in lung VSMC differentiation. The role of the miR-29 family is also indicated in TGF-β-modulated cell proliferation, differentiation, and apoptosis in PA vasculature. In particular, elevated miR-29 observed in the heritable form of PAH (HPAH) modulates cellular energy metabolism, contributing to PAH pathogenesis.[27,34–36] Based on the literature, we focused on hsa-miR-210 and hsa-miR-29 to verify whether they were directly bound by hsa_circNFXL1_009. A luciferase assay proved that hsa-miR-29b-2-5p was one direct target for hsa_circNFXL1_009 sponging.

Given views of downstream mRNA, more than 800 targets for hsa-miR-29b-2-5p were predicted in the miRNA database (data not shown). Rather than randomly ruling out other potential targets, we focused on KCNB1, a classic, top-ranking predicted biomarker of PAH. Downregulated expression levels of K⁺ channels and decreased K⁺ currents play an essential role in sustained pulmonary

vasoconstriction and vascular remodeling in the pathogenesis of PAH.[32] *KCNB1*-encoded Kv2.1 is one major delayed-rectifier, voltage-gated K^+ channel, playing an essential role in the membrane potential of arterial smooth muscle. Loss of Kv2.1 in PASMC contributes to the pathogenesis of PAH by causing a sustained depolarization, thereby increasing intracellular Ca^{2+}, which is highly related to vascular tone and proliferation rate.[32,37] Therefore, we performed molecular and electrophysiological studies to examine whether PAH-related hsa_circNFXL1_009 can regulate the expression of the K^+ channel (i.e., KCNB1) and K^+ currents in hPASMCs. As expected, hsa_circNFXL1_009 overexpression increased *KCNB1*gene expression in mRNA level and whole-cell K^+ currents in hPASMCs, indicating an essential role of hsa_circNFXL1_009 in PAH by regulating K^+ channel activation. Clearly, how circNFXL1-miR-29b-KCNB1 regulated K^+ channel activities was still unclear. Other unidentified targets may contribute to the pathological process of PAH. The underlying mechanisms still need to be studied further. Nevertheless, the aberrant expression of the global circRNAs in COPD-PAH reveals that the post-transcriptional gene expression regulated by circRNAs was an essential step in PAH pathogenesis, and the roles of hsa_circNFXL1_009 in hypoxic cell K^+ activation, proliferation, anti-apoptosis, and migration were also indicated in PAH progression. All of these findings indicated a new clue for the PAH study that hsa_circNFXL1_009 was associated with HPVR via sponging the miR-29b-KCNB1 axis.

Recently, Miao et al.[38] demonstrated a dysregulated circRNA pattern in chronic thromboembolic pulmonary hypertension (CTEPH) patients, and they proved hsa_circ_0002062 and hsa_circ_0022342 to be key circRNAs for CTEPH development. Zhou et al.[24] further studied their role in PAH and proved that in human and rat PASMCs, hsa_circ_0016070 transfection can increase the cell viability and decrease the number of cells arrested in the G_1/G_0 phase, indicating its pro-proliferation effects on PASMCs and association with the vascular remodeling in PAH. In animal models, Wang et al.[39] have profiled the circRNA expression in hypoxia-induced PAH mice models, although there were no common circRNAs between their study and ours, which may be a result of experimental species. It is noteworthy that hsa_circNFXL1_009 does not have a mouse homology. We looked into seven databases (circBank, circAtlas, CIRCpedia, circRNADb, exoRBase, circBase, and TSCD), which contain about 835,785 human cirRNAs and 270,424 mouse circRNAs, but we failed to find a mouse homology, indicating that the unknown mouse circRNAs still need to be found in the future. Limited by the unknown mouse cirRNAs, we could not perform additional studies in the mouse models/cell lines. However, the hsa_circNFXL1_009-sponged hsa-miR-29b-2-5p is highly homologous to mouse mmu-miR-29b-2-5p, which is targeted by mouse Kcnb1. Notably, the binding site of hsa/mmu-miR-29b-2-5p and KCNB1/Kcnb1 is highly conserved in humans and mice (Figure 6A; Table S2), indicating the regulation of hsa_circNFXL1_009 in a mouse model. With continuing progress in the studies of circRNAs, the value of hsa_circNFXL1_009 in other species will arise in the near future.

Our results from the GO process identified the regulation of MCP-1 production in BP, while transferase activity in MF. Monocyte chemo-attractant protein-1 (MCP-1) is a pro-inflammatory chemokine involved in immunoregulatory and inflammatory processes. Recent studies have indicated that MCP-1 is elevated in PAH patients, contributing to the inflammatory processes of PAH.[40,41] Meanwhile, transferase is one group of enzymes that can transfer specific functional modifications from one molecule to another. Different transferases are involved in a wide variety of biochemical pathways and critical BPs. In the monocrotaline (MCT)-induced PAH rat model, nicotinamide *N*-methyltransferase (NNMT) activity increases progressively, as does the activation of the NNMT-MNA pathway in rats and humans.[42] Concerning the KEGG pathway, the NF-κB signaling pathway shows its importance in PAH progression. By targeting the BMPR2-Id-Notch-3 gene axis, NF-κB inactivation can attenuate the inflammatory response, reduce endothelial cell apoptosis, and reverse endothelial-to-mesenchymal transition in the MCT-induced mice model. hsa_circNFXL1_009 may participate in affecting the airways and lung parenchyma in COPD, providing a novel therapeutic intervention target in PAH.[43,44]

Despite these encouraging findings, there are still limitations in the present study. First, due to ethical considerations, inaccurate and noninvasive methods were used for PAH-COPD diagnosis instead of invasive right heart catheterization (RHC) measurements. Assessment of PAH was performed by echocardiography with systolic pulmonary arterial pressure (sPAP) higher than 38 mmHg and exclusion of associated left heart disease. Second, as the differentially expressed circRNAs were identified in a small size of the population without univariate and multivariate analyses, the potential predictive power should be considered carefully. More extensive clinical studies should be performed in a new set of patients to validate the predictive ability of hsa_circNFXL1_009 on the progression of PAH. Last, the function of hsa_circNFXL1_009 sponging the miR-29b-KCNB1 axis needs to be confirmed in further studies. Possible functions such as mRNA alternative splicing, transcriptional regulation, and sequestering translation also need to be ascertained in further functional studies.

In conclusion, our present study provides evidence for aberrant expression of circRNAs in PAH-COPD patients and the role of hsa_circNFXL1_009 in hypoxic hPASMCs. Decreased levels of hsa_circNFXL1_009 might drive the excessive proliferation, apoptotic resistance, and migration of PASMCs, resulting in remodeling of pulmonary vessels in the development of PAH. Meanwhile, decreased expression of hsa_circNFXL1_009 might contribute to the observed decreased K^+ channel activities in PAH by sponging the miR-29b-2-5p-KCNB1 axis. Thus, hsa_circNFXL1_009 might be useful for the diagnosis of PAH patients and considered as a potential therapeutic molecule to inhibit PAH development.

MATERIALS AND METHODS
Ethics
The study procedure was approved by the Medical Ethics Committee of Harbin Medical University (IRB3011619). All subjects who

participated in this study have been informed of the objectives of the project. Consent forms were obtained before the study.

Subjects

Subjects with COPD were enrolled at the Department of Cardiology at The Fourth Affiliated Hospital of Harbin Medical University from January 2015 to October 2018. sPAP was examined by echocardiography, and an sPAP higher than 38mmHg was diagnosed as PAH.[45] Patients with PAH that were classified as groups 1, 2, 4, and 5, as well as patients with connective tissue disease, congenital heart diseases, diabetes, and lung diseases, were excluded from the study. Echocardiograms in patients with PAH-COPD were obtained using a Philips iE33 color Doppler ultrasound system (Philips, the Netherlands). Heart rate and blood pressure were measured just before the study. The electrocardiogram measurements were operated under the current guidelines of the American Society of Echocardiography by the same expert ultrasonographer. The data were independently analyzed by two investigators and stored on DVDs. sPAP was calculated by the combined peak of tricuspid regurgitation velocity (V) and the right atrial pressure (RAP) in the equation of $4(V^2)$ + RAP.[45] Age- and sex-matched healthy control groups were recruited at the Department of Health from The Second Affiliated Hospital of Harbin Medical University. Finally, 21 cases of PH-COPD and 21 healthy controls were collected for this study. Whole-blood samples were obtained in EDTA-coated blood collection tubes from all subjects.

RNA isolation

A total of 2 mL of whole blood was extracted in Vacuette K2 EDTA gel tubes (Greiner Bio-One, Austria), and total RNA from each subject was isolated with TRI Reagent BD (Molecular Research Center) using the manufacturer's protocol. The concentration, purity, integrity, and genome DNA contamination of total RNA samples were analyzed with a NanoDrop ND-1000 (Thermo Scientific, USA) and denaturing agarose gel electrophoresis.

circRNA array

The circRNA array analysis was performed by Kang-Chen Biotech (Shanghai, China). Briefly, whole-blood samples from three pairs of subjects were randomly selected for the Arraystar human circRNA array analysis. The linear RNAs were removed by RNase R (Epicenter) to enrich circRNAs. The circRNAs were transcribed into fluorescent cRNA and hybridized onto the Arraystar human circRNA array (8 ×15K, Arraystar) using a random priming method. The arrays were then scanned by an Agilent G2505C scanner followed by washing. Array images and data analysis were performed using Agilent Feature Extraction software (version 11.0.1.1) and the R software package. Differentially expressed circRNAs with a p value <0.05 between the two groups were exhibited by a volcano plot and hierarchical clustering.

qRT-PCR validation

The top 20 most differentially expressed circRNAs from array analysis were further validated by qRT-PCR on whole-blood samples from 21 pairs of subjects. Total RNA was reverse transcribed by a high-capacity cDNA reverse transcription kit (Applied Biosystems,

Life Technologies, NewYork, NY, USA), and the circRNAs were amplified using Fast SYBR Green master mix (Applied Biosystems, Life Technologies, New York, NY, USA). All procedures were performed using the manufacturer's instructions. Divergent primers for each circRNA are presented in Table S1. β-actin was used as an internal control. The relative expression of each group was analyzed using the $2^{-\Delta\Delta Ct}$ method.

Cell culture

HEK293 cells (CRL-1573; American Type Culture Collection, Manassas, VA, USA) were cultured in complete DMEM supplied with fetal bovine serum (FBS) (10%), streptomycin (1%), and penicillin (1%) in a humidified incubator with CO_2 (5%) at 37°C. Two to four generations were used for luciferase assays. All primary cell lines of hPASMCs were purchased from Procell Life Science & Technology (Wuhan, China; CP-H003), exhibiting a contractile phenotype. At least four primary hPASMCs cell lines were used for this study. Each primary cell line for hPASMCs can only be used for fewer than five generations to indicate reliable positive results. Cell culture was performed by the manufacturer's instructions and followed by our previous studies.[46] Briefly, the primary hPASMCs were cultured in smooth muscle cell medium (SMCM, Zhong Qiao Xin Zhou Biotechnology, Shanghai, China) in a CO_2 (5%) atmosphere at 37°C. For hypoxic culture, hPASMCs were exposed to CO_2 (5%)/O_2 (3%)/balance of N_2 for 48 h. We only use three to five generations with an α-smooth muscle actin (α-SMA) phenotype to assure the reproductivity.

Immunocytochemistry

hPASMCs were plated onto 35-mm glass-bottom Petri dishes and grown to 50%–70% confluence. Cells were fixed with 4% polyformaldehyde before the membrane breaking with 0.3% Triton X-100. After blocking with 5% BSA, hPASMCs were incubated with the anti-α-SMA antibody (fluorescein isothiocyanate [FITC]) (Abcam, ab8211, 1:200, diluted with BSA) overnight at 4°C. On the following day, after washing out the excessive antibody by PBS, the nuclei were stained with 4',6-diamidino-2-phenylindole (DAPI) (Beyotime, A1107, 1:1,000, diluted with PBS) and the images were captured with a confocal microscope (Nikon, C1).

RNA FISH

The hPASMCs were cultured on 24-well plates. The expression of hsa_circNFXL1_009 was detected by an RNA FISH kit (Boster Bio-engineering, Wuhan, China) on 4% paraformaldehyde-fixed hPASMCs. The cyanine dye-labeled probes for hsa_circNFXL1_009 were designed and synthesized by GenePharma (Shanghai, China). The nuclei were stained with DAPI. Images were captured by microscopy (Olympus IX71, Nikon Instruments, Japan) and analyzed with imaging software (NIS-Elements, Nikon Instruments, Japan).

Construction of hsa_circNFXL1_009 expression vector

The mature hsa_circNFXL1_009 sequence was cloned with a primer pair (forward, 5'-CGGAATTCTAATACTTTCAGATGGAGATA CACGTGAATTAGA-3'; reverse, 5'-CGGGATCCAGTTGTTCTT ACCAAGGCCAGGGACAATCTTTCTTTC-3') and inserted into

pLC5-ciR, which contained a specific frame for circRNA circularization (Geneseed Biotech, Guang Zhou, China). Circularization was assayed by RT-PCR with divergent primers, and the junction sites were confirmed by Sanger sequencing. The efficiency of a vector containing hsa_circNFXL1_009 was evaluated by qRT-PCR with divergent primers.

Cell transfection

After serum deprivation, the cells were co-transfected with 1 μg of plasmids/oligonucleotides using Lipofectamine agents (Thermo Scientific, USA) according to the manufacturer's instructions. After 4 h, the cells were switched to SMCM/complete DMEM with FBS (10%) and cultured for another 24–48 h.

Cell viability

hPASMCs were cultured in 96-well plates transfected with different groups. After a 48-h culture, cell proliferation capacity was evaluated by an EdU cell proliferation kit with tetramethylbenzidine (TMB) (Beyotime Biotechnology, Shanghai, China). Briefly, the cells were treated as indicated, and EdU was added to replace thymidine during DNA synthesis. With click reactions, EdU was labeled with biotin, allowing the proliferation of cells to be combined by streptavidin-horseradish peroxidase (HRP) and detected by TMB substrate. The plates were read using a spectrophotometer microplate reader (PowerWave XS2, BioTek Instruments, USA) with a single wavelength of 370 nm.

Wound-healing assay

The hPASMCs were cultured on 24-well plates. After transfection, the cell motility and migration were compared using a wound-healing assay. Briefly, a "wound" was created by a pipette in a cell monolayer and captured by microscopy at the beginning. After a 48-h culture, the images were recaptured and compared by calculating the migration rate of the cells.

TUNEL assay

The apoptotic hPASMCs were detected using a terminal deoxynucleotidyltransferase (TdT)-mediated one-step TUNEL apoptosis assay kit (Beyotime Biotechnology, Shanghai, China). After transfection, the hPASMCs were fixed as above and permeated by 0.1% Triton X-100 for 2 min on ice. After a 1-h incubation with TUNEL working solution at 37°C, the FITC-labeled cells were imaged at 488 nm excitation and 530 nm emission by a fluorescence microscope (Nikon-OLYMPUS IX71, Nikon Instruments, Japan). The cells with green fluorescence were calculated as apoptotic cells.

Luciferase assay

The WT sequence of hsa_circNFXL1_009 was synthesized and subcloned into the downstream of the Renilla luciferase reporter gene of the psiCHECK-2 expression reporter vector and named as circNFXL1-WT (Hanbio Biotechnology, Shanghai, China). The sequence of hsa_circNFXL1_009 with four mutation sites in positions 100, 102, 104, and 106 was synthesized and subcloned into the downstream of psiCHECK-2 and named as circNFXL1-M1. The sequence

of hsa_circNFXL1_009 with four mutation sites in positions 58, 60, 62, and 64 was synthesized and subcloned into the downstream of psiCHECK-2 and named as circNFXL1-M2. Double-stranded nucleotides were designed to mimic endogenous mature hsa-miR-29b-2-5p (miRBase: MIMAT0004515) and hsa-miR-210-5p (miRBase: MIMAT0026475), which were synthesized by GenePharma. A scrambled RNA was used as a negative control (NC). The mixture of circNFXL1-WT/circNFXL1-M1/circNFXL1-M2 and hsa-miR-29b-2-5p/hsa-miR-210-5p/NC was co-transfected into HEK293 cells. Luciferase activities were measured with a double-luciferase reporter assay kit (TransGen Biotech, Beijing, China) on a luminometer (GloMax 20/20, Promega, USA) after 1-day culture.

Whole-cell patch clamp

The whole-cell K^+ current was recorded using an EPC10 USB patch-clamp amplifier (HEKA Electronik). The generation of voltage pulse and collection of data were performed using Patchmaster 10 software (HEKA Electronik). The voltage pulse protocol applied 10-mV voltage steps with 200-ms duration, from −60 to 90 mV. The holding potential was −70 mV, which is equal to the reversal potential for potassium. The extracellular solution contained 141 mM NaCl, 4.7 mM KCl, 1.8 mM $CaCl_2$, 1.2 mM $MgCl_2$, 10 mM HEPES, and 10 mM glucose (pH 7.4). The pipette solution contained 135 mM KCl, 4 mM $MgCl_2$, 10 mM HEPES, 10 mM EGTA, and 5 mM Na_2ATP (pH 7.2).

ceRNA network construction

With miRNA response elements (MREs), the ceRNA hypothesis describes that RNA transcripts are interrelated and interact with each other by competitive binding to miRNAs.[47,48] The targets/miRNAs were analyzed using home-made prediction software to find the potential targets of miRNAs based on TargetScan and miRanda.[49–51] Through merging the commonly targeted miRNAs, we constructed a circRNA-miRNA-mRNA interaction network of hsa_circNFXL1_009. The functional pathways of top-ranked MREs were analyzed by DIANA-miRPath tools.

Functional group analysis

The molecular functional roles of the circRNA-target genes profiles were analyzed using GO (http://www.geneontology.org/). The ontology covers three domains: BP, CC, and MF. The p value produced by topGO denoted the significance of GO term enrichment in the circRNA-miRNA-targeted genes. Pathway analysis was identified by KEGG. The p value (EASE score, Fisher's p value, or hypergeometric p value) denoted the significance of the pathway relevant to PAH-COPD. The p value cutoff was 0.05.

Statistical analysis

All data were expressed as mean ± SEM (standard error of the mean). Mean values, standard deviations, and statistical differences were examined with Excel 2013 (Microsoft). The differently expressed circRNAs having a fold change >1.5 and a p value <0.05 were selected as candidates. Using Prism 8.0 and SPSS 2.0, ROC curves and the AUC value, as well as the 95% CIs, were acquired to assess the

performance of validated circRNAs in predicting potential association with PAH. Comparisons of data were acquired by one-way ANOVA followed by a Bonferroni post hoc test or Student's t test. When p ≤0.05, the mean difference was significant.

SUPPLEMENTAL INFORMATION

Supplemental Information can be found online at https://doi.org/10.1016/j.omtn.2020.09.029.

AUTHOR CONTRIBUTIONS

Investigation, X.J., Y.X., L.L., and J.D.; formal analysis, M.G., Y.S., S.L., D.Y., and X.Z.; conceptualization, X.J. and S.-S.L; writing – original draft, X.J. and S.-S.L.; writing – review & editing, X.J. and S.-S.L.; funding acquisition, X.J. and S.-S.L.

DECLARATION OF INTERESTS

The authors declare no competing interests.

REFERENCES

1. Dodson, M.W., Brown, L.M., and Elliott, C.G. (2018). Pulmonary arterial hypertension. Heart Fail. Clin. 14, 255–269.

2. Schermuly, R.T., Ghofrani, H.A., Wilkins, M.R., and Grimminger, F. (2011). Mechanisms of disease: pulmonary arterial hypertension. Nat. Rev. Cardiol. 8, 443–455.

3. Hayabuchi, Y. (2017). The action of smooth muscle cell potassium channels in the pathology of pulmonary arterial hypertension. Pediatr. Cardiol. 38, 1–14.

4. Wakasugi, T., Shimizu, I., Yoshida, Y., Hayashi, Y., Ikegami, R., Suda, M., Katsuumi, G., Nakao, M., Hoyano, M., Kashimura, T., et al. (2019). Role of smooth muscle cell p53 in pulmonary arterial hypertension. PLoS ONE 14, e0212889.

5. Sylvester, J.T., Shimoda, L.A., Aaronson, P.I., and Ward, J.P. (2012). Hypoxic pulmonary vasoconstriction. Physiol. Rev. 92, 367–520.

6. Kylhammar, D., and Rådegran, G. (2017). The principal pathways involved in the in vivo modulation of hypoxic pulmonary vasoconstriction, pulmonary arterial remodelling and pulmonary hypertension. Acta Physiol. (Oxf.) 219, 728–756.

7. Kristensen, L.S., Andersen, M.S., Stagsted, L.V.W., Ebbesen, K.K., Hansen, T.B., and Kjems, J. (2019). The biogenesis, biology and characterization of circular RNAs. Nat. Rev. Genet. 20, 675–691.

8. Lasda, E., and Parker, R. (2014). Circular RNAs: diversity of form and function. RNA 20, 1829–1842.

9. Memczak, S., Jens, M., Elefsinioti, A., Torti, F., Krueger, J., Rybak, A., Maier, L., Mackowiak, S.D., Gregersen, L.H., Munschauer, M., et al. (2013). Circular RNAs are a large class of animal RNAs with regulatory potency. Nature 495, 333–338.

10. Hansen, T.B., Jensen, T.I., Clausen, B.H., Bramsen, J.B., Finsen, B., Damgaard, C.K., and Kjems, J. (2013). Natural RNA circles function as efficient microRNA sponges. Nature 495, 384–388.

11. Zhang, Y., Xue, W., Li, X., Zhang, J., Chen, S., Zhang, J.L., Yang, L., and Chen, L.L. (2016). The biogenesis of nascent circular RNAs. Cell Rep. 15, 611–624.

12. Du, W.W., Yang, W., Chen, Y., Wu, Z.K., Foster, F.S., Yang, Z., Li, X., and Yang, B.B. (2017). Foxo3 circular RNA promotes cardiac senescence by modulating multiple factors associated with stress and senescence responses. Eur. Heart J. 38, 1402–1412.

13. Liang, D., and Wilusz, J.E. (2014). Short intronic repeat sequences facilitate circular RNA production. Genes Dev. 28, 2233–2247.

14. Salzman, J., Gawad, C., Wang, P.L., Lacayo, N., and Brown, P.O. (2012). Circular RNAs are the predominant transcript isoform from hundreds of human genes in diverse cell types. PLoS ONE 7, e30733.

15. Liu, Q., Zhang, X., Hu, X., Dai, L., Fu, X., Zhang, J., and Ao, Y. (2016). Circular RNA related to the chondrocyte ECM regulates MMP13 expression by functioning as a miR-136 "sponge" in human cartilage degradation. Sci. Rep. 6, 22572.

16. Bachmayr-Heyda, A., Reiner, A.T., Auer, K., Sukhbaatar, N., Aust, S., Bachleitner-Hofmann, T., Mesteri, I., Grunt, T.W., Zeillinger, R., and Pils, D. (2015). Correlation of circular RNA abundance with proliferation—exemplified with colorectal and ovarian cancer, idiopathic lung fibrosis, and normal human tissues. Sci. Rep. 5, 8057.

17. Mehta, S.L., Pandi, G., and Vemuganti, R. (2017). Circular RNA expression profiles alter significantly in mouse brain after transient focal ischemia. Stroke 48, 2541–2548.

18. Li, Y., Zheng, Q., Bao, C., Li, S., Guo, W., Zhao, J., Chen, D., Gu, J., He, X., and Huang, S. (2015). Circular RNA is enriched and stable in exosomes: a promising biomarker for cancer diagnosis. Cell Res. 25, 981–984.

19. Akhter, R. (2018). Circular RNA and Alzheimer's disease. Adv. Exp. Med. Biol. 1087, 239–243.

20. Sand, M., Bechara, F.G., Sand, D., Gambichler, T., Hahn, S.A., Bromba, M., Stockfleth, E., and Hessam, S. (2016). Circular RNA expression in basal cell carcinoma. Epigenomics 8, 619–632.

21. Guo, L.L., Song, C.H., Wang, P., Dai, L.P., Zhang, J.Y., and Wang, K.J. (2015). Competing endogenous RNA networks and gastric cancer. World J. Gastroenterol. 21, 11680–11687.

22. Zhong, Z., Lv, M., and Chen, J. (2016). Screening differential circular RNA expression profiles reveals the regulatory role of circTCF25-miR-103a-3p/miR-107-CDK6 pathway in bladder carcinoma. Sci. Rep. 6, 30919.

23. Liang, H.F., Zhang, X.Z., Liu, B.G., Jia, G.T., and Li, W.L. (2017). Circular RNA circ-ABCB10 promotes breast cancer proliferation and progression through sponging miR-1271. Am. J. Cancer Res. 7, 1566–1576.

24. Zhou, S., Jiang, H., Li, M., Wu, P., Sun, L., Liu, Y., Zhu, K., Zhang, B., Sun, G., Cao, C., and Wang, R. (2019). Circular RNA hsa_circ_0016070 is associated with pulmonary arterial hypertension by promoting PASMC proliferation. Mol. Ther. Nucleic Acids 18, 275–284.

25. Gou, D., Ramchandran, R., Peng, X., Yao, L., Kang, K., Sarkar, J., Wang, Z., Zhou, G., and Raj, J.U. (2012). miR-210 has an antiapoptotic effect in pulmonary artery smooth muscle cells during hypoxia. Am. J. Physiol. Lung Cell. Mol. Physiol. 303, L682–L691.

26. Tang, H., Ayon, R.J., and Yuan, J.X. (2015). New insights into the pathology of pulmonary hypertension: implication of the miR-210/ISCU1/2/Fe-S axis. EMBO Mol. Med. 7, 689–691.

27. Cushing, L., Costinean, S., Xu, W., Jiang, Z., Madden, L., Kuang, P., Huang, J., Weisman, A., Hata, A., Croce, C.M., and Lü, J. (2015). Disruption of miR-29 leads to aberrant differentiation of smooth muscle cells selectively associated with distal lung vasculature. PLoS Genet. 11, e1005238.

28. Kameny, R.J., He, Y., Zhu, T., Gong, W., Raff, G.W., Chapin, C.J., Datar, S.A., Boehme, J.T., Hata, A., and Fineman, J.R. (2018). Analysis of the microRNA signature driving adaptive right ventricular hypertrophy in an ovine model of congenital heart disease. Am. J. Physiol. Heart Circ. Physiol. 315, H847–H854.

29. Bonnet, S., and Archer, S.L. (2007). Potassium channel diversity in the pulmonary arteries and pulmonary veins: implications for regulation of the pulmonary vasculature in health and during pulmonary hypertension. Pharmacol. Ther. 115, 56–69.

30. Archer, S.L., Souil, E., Dinh-Xuan, A.T., Schremmer, B., Mercier, J.C., El Yaagoubi, A., Nguyen-Huu, L., Reeve, H.L., and Hampl, V. (1998). Molecular identification of the role of voltage-gated K+ channels, Kv1.5 and Kv2.1, in hypoxic pulmonary

vasoconstriction and control of resting membrane potential in rat pulmonary artery myocytes. J. Clin. Invest. 101, 2319–2330.

31. Michelakis, E.D., Dyck, J.R., McMurtry, M.S., Wang, S., Wu, X.C., Moudgil, R., Hashimoto, K., Puttagunta, L., and Archer, S.L. (2001). Gene transfer and metabolic modulators as new therapies for pulmonary hypertension. Increasing expression and activity of potassium channels in rat and human models. Adv. Exp. Med. Biol. 502, 401–418.

32. Moudgil, R., Michelakis, E.D., and Archer, S.L. (2006). The role of K+ channels in determining pulmonary vascular tone, oxygen sensing, cell proliferation, and apoptosis: implications in hypoxic pulmonary vasoconstriction and pulmonary arterial hypertension. Microcirculation 13, 615–632.

33. Jeck, W.R., Sorrentino, J.A., Wang, K., Slevin, M.K., Burd, C.E., Liu, J., Marzluff, W.F., and Sharpless, N.E. (2013). Circular RNAs are abundant, conserved, and associated with ALU repeats. RNA 19, 141–157.

34. Chou, J., Lin, J.H., Brenot, A., Kim, J.W., Provot, S., and Werb, Z. (2013). GATA3 suppresses metastasis and modulates the tumour microenvironment by regulating microRNA-29b expression. Nat. Cell Biol. 15, 201–213.

35. Zhou, L., Wang, L., Lu, L., Jiang, P., Sun, H., and Wang, H. (2012). Inhibition of miR-29 by TGF-beta-Smad3 signaling through dual mechanisms promotes transdifferentiation of mouse myoblasts into myofibroblasts. PLoS ONE 7, e33766.

36. Chen, X., Talati, M., Fessel, J.P., Hemnes, A.R., Gladson, S., French, J., Shay, S., Trammell, A., Phillips, J.A., Hamid, R., et al. (2016). Estrogen metabolite 16α-hydroxyestrone exacerbates bone morphogenetic protein receptor type II-associated pulmonary arterial hypertension through microRNA-29-mediated modulation of cellular metabolism. Circulation 133, 82–97.

37. Morales-Cano, D., Menendez, C., Moreno, E., Moral-Sanz, J., Barreira, B., Galindo, P., Pandolfi, R., Jimenez, R., Moreno, L., Cogolludo, A., et al. (2014). The flavonoid quercetin reverses pulmonary hypertension in rats. PLoS ONE 9, e114492.

38. Miao, R., Wang, Y., Wan, J., Leng, D., Gong, J., Li, J., Liang, Y., Zhai, Z., and Yang, Y. (2017). Microarray expression profile of circular RNAs in chronic thromboembolic pulmonary hypertension. Medicine (Baltimore) 96, e7354.

39. Wang, J., Zhu, M.C., Kalionis, B., Wu, J.Z., Wang, L.L., Ge, H.Y., Chen, C.C., Tang, X.D., Song, Y.L., He, H., and Xia, S.J. (2018). Characteristics of circular RNA expression in lung tissues from mice with hypoxia-induced pulmonary hypertension. Int. J. Mol. Med. 42, 1353–1366.

40. Zhang, Y., Zhang, F., Wang, X., Xie, Y., Du, J., Lu, P., and Wang, W. (2015). Sequential and timely transfection of hepatocyte growth factor and monocyte chemotactic protein-1 ameliorates hyperkinetic pulmonary artery hypertension in rabbits. J. Thorac. Cardiovasc. Surg. 150, 634–643.e2.

41. Itoh, T., Nagaya, N., Ishibashi-Ueda, H., Kyotani, S., Oya, H., Sakamaki, F., Kimura, H., and Nakanishi, N. (2006). Increased plasma monocyte chemoattractant protein-1 level in idiopathic pulmonary arterial hypertension. Respirology 11, 158–163.

42. Fedorowicz, A., Mateuszuk, Ł., Kopec, G., Skórka, T., Kutryb-Zając, B., Zakrzewska, A., Walczak, M., Jakubowski, A., Łomnicka, M., Słomińska, E., and Chlopicki, S. (2016). Activation of the nicotinamide N-methyltransferase (NNMT)-1-methylnicotinamide (MNA) pathway in pulmonary hypertension. Respir. Res. 17, 108.

43. Hosokawa, S., Haraguchi, G., Sasaki, A., Arai, H., Muto, S., Itai, A., Doi, S., Mizutani, S., and Isobe, M. (2013). Pathophysiological roles of nuclear factor kappaB (NF-κB) in pulmonary arterial hypertension: effects of synthetic selective NF-κB inhibitor IMD-0354. Cardiovasc. Res. 99, 35–43.

44. Li, L., Wei, C., Kim, I.K., Janssen-Heininger, Y., and Gupta, S. (2014). Inhibition of nuclear factor-κB in the lungs prevents monocrotaline-induced pulmonary hypertension in mice. Hypertension 63, 1260–1269.

45. Rudski, L.G., Lai, W.W., Afilalo, J., Hua, L., Handschumacher, M.D., Chandrasekaran, K., Solomon, S.D., Louie, E.K., and Schiller, N.B. (2010). Guidelines for the echocardiographic assessment of the right heart in adults: a report from the American Society of Echocardiography endorsed by the European Association of Echocardiography, a registered branch of the European Society of Cardiology, and the Canadian Society of Echocardiography. J. Am. Soc. Echocardiogr. 23, 685–713, quiz 786–788.

46. Li, S., Ran, Y., Zhang, D., Chen, J., Li, S., and Zhu, D. (2013). MicroRNA-138 plays a role in hypoxic pulmonary vascular remodelling by targeting Mst1. Biochem. J. 452, 281–291.

47. Salmena, L., Poliseno, L., Tay, Y., Kats, L., and Pandolfi, P.P. (2011). A ceRNA hypothesis: the Rosetta Stone of a hidden RNA language? Cell 146, 353–358.

48. Tay, Y., Rinn, J., and Pandolfi, P.P. (2014). The multilayered complexity of ceRNA crosstalk and competition. Nature 505, 344–352.

49. Garcia, D.M., Baek, D., Shin, C., Bell, G.W., Grimson, A., and Bartel, D.P. (2011). Weak seed-pairing stability and high target-site abundance decrease the proficiency of lsy-6 and other microRNAs. Nat. Struct. Mol. Biol. 18, 1139–1146.

50. Grimson, A., Farh, K.K., Johnston, W.K., Garrett-Engele, P., Lim, L.P., and Bartel, D.P. (2007). MicroRNA targeting specificity in mammals: determinants beyond seed pairing. Mol. Cell 27, 91–105.

51. Enright, A.J., John, B., Gaul, U., Tuschl, T., Sander, C., and Marks, D.S. (2003). MicroRNA targets in Drosophila. Genome Biol. 5, R1.